Gusts caused by high-speed trains in confined spaces and tunnels

Baker, C.J.; Gilbert, T.; Quinn, A.

DOI:
10.1016/j.jweia.2013.07.015

Document Version
Early version, also known as pre-print

Citation for published version (Harvard):
Baker, CJ, Gilbert, T & Quinn, A 2013, 'Gusts caused by high-speed trains in confined spaces and tunnels', *Journal of Wind Engineering and Industrial Aerodynamics*, vol. 121, pp. 39-48.
https://doi.org/10.1016/j.jweia.2013.07.015

Elsevier Editorial System(tm) for Journal of Wind Engineering & Industrial Aerodynamics
Manuscript Draft

Manuscript Number: INDAER-D-13-00018R2

Title: Gusts caused by high-speed trains in confined spaces and tunnels

Article Type: Full Length Article

Keywords: High speed trains; Air velocities; Slipstreams; Wakes; Gusts; Walls; Tunnels; Confined spaces

Corresponding Author: Mr. Tim Gilbert,

Corresponding Author's Institution:

First Author: Tim Gilbert

Order of Authors: Tim Gilbert; Christopher Baker, Professor; Andrew Quinn, PhD

- We measure the velocity around a high-speed train in various confined spaces.
- Moving-model experiments were carried out with a simplified ICE2.
- Cases included the open air, walls, short tunnels, and a partially enclosed tunnel.
- A pressure-driven piston effect causes high gust magnitudes in tunnels.
- Tunnel length and cross-sectional area affect the gust magnitudes.
- High lateral and vertical velocities occur in the partially-enclosed tunnel.

Gusts caused by high-speed trains in confined spaces and tunnels

T Gilbert*, CJ Baker, A Quinn

Birmingham Centre for Railway Research and Education, School of Civil Engineering, University of Birmingham

* Corresponding author: School of Civil Engineering, The University of Birmingham, Edgbaston, Birmingham, West Midlands, B15 2TT, UK. Email: tkg614@bham.ac.uk. Tel: +447563791094.

Keywords: High speed trains; Air velocities; Slipstreams; Wakes; Gusts; Walls; Tunnels; Confined spaces.

MEMO: Please consider for publication for a possible special issue of WES 2012 (Wind Engineering Society 2012 Conference, University of Southampton, UK, 10-12 September 2012)

Abstract

Little is known of the behaviour of transient air velocities and dynamic pressure loads generated by high-speed trains in confined spaces, or whether current methodologies for assessing transient gust loads in open spaces can be used in confined spaces. Experiments have been carried out in which a moving-model high-speed train passed walls, a partially-enclosed tunnel, and single-track tunnels with a variety of cross-sectional areas and lengths. An open air control experiment has also been carried out. The train model was a simplified 1/25 scale four-carriage ICE2 train travelling at 32m/s. Cobra Probes measured the three-dimensional air velocity components at various positions inside the structures. The results show that the peak gust magnitudes increase in all confined cases compared to the open air. In tunnels, a 'piston effect' appears to have been a dominant cause of the increases in the peak gust magnitudes, as well as prolonged winds occurring before and after the train passed the probes. The tunnel length impacted considerably on the flow characteristics, and the partially-enclosed tunnel showed further increases in the gusts due to high lateral and vertical velocities.

1. Introduction

Passing trains impose transient slipstream gust loads on trackside workers and permanent or temporary trackside furniture. Codes of practice require that the maximum gust load generated by a passing train is treated as a design load. Research by Sterling et al. (2008) into the fundamentals of transient slipstreams of high-speed trains found that the flow field in the open air can be defined by four regions, including: a nose region in which an inviscid velocity fluctuation occurs; a boundary layer region in which a turbulent and highly three-dimensional boundary layer develops along the length of the train on all sides; a near-wake region which is dominated by large-scale unsteady flow structures; and a far-wake region in which the slipstream velocity decays gradually. The relationship between the train's aerodynamic shape and the transient slipstream has been studied in Baker et al. (2013a) and Baker et al. (2013b). The German Railways (DB) ICE2 train is the most widely and deeply researched high-speed train for transient aerodynamics, with many different assessment methods used, including: moving-model tests on straight tracks (Baker et al., 2001; Temple and Dalley, 2001), and rotating tracks (Del Valle, 2012); full-scale tests (Baker et al., 2013a; Baker et al., 2013b; Temple and Dalley, 2001); and CFD simulations, for example those which have used the 'simplified ICE2' or 'ATM' geometries (Krajnovic, 2009; Krajnovic et al., 2009; Hemida et al., 2012; Muld, 2012).

Until now, little attention has been devoted to assessing transient slipstream velocity gusts in 'confined spaces'. These include tunnels (defined as 20m or longer by code of practice CEN (2006)), partially-enclosed tunnels which are slightly open to the atmosphere, and vertical

surfaces running parallel to the tracks such as noise barriers. CEN (2003) provides a summary of the factors affecting slipstreams in tunnels - 'the induced flow velocity depends on the train speed, the blockage ratio [the train area divided by the tunnel area], the length of the train, and of the tunnel respectively, the roughnesses [sic] of the train and the tunnel wall respectively, and on the initial air speed in the tunnel'. It was stated that an upcoming code of practice would discuss the issues further. However this has not yet been fulfilled. A German national regulation (Deutsche Bahn, 2003) includes a relationship between the maximum air velocity in tunnels, the train speed, and the ratio of the cross-sectional areas of the train and tunnel, but its use may lead to over-predictions of air velocity, as was found in a comparison between prediction and experiment reported in Busslinger et al. (2007).

This investigation aims to establish how different configurations of confining infrastructure affect the transient slipstream velocities and maximum gust loads caused by a passing train. A parametric experimental study has been undertaken at the 'TRAIN Rig' moving-model facility in Derby (UK), which is owned and operated by the University of Birmingham. The experiments involved firing a simplified ICE2 model train past various instrumented trackside structures. This paper compares the flow patterns and maximum velocities with various geometric parameters associated with the trackside structures. The methodology is described in Section 2. In Section 3, the reliability of the data is checked against results from previous studies and duplicated experiments and measurements. The data is presented and analysed in Sections 4 and 5.

2 Methodology

2.1 TRAIN Rig, simplified ICE2 model and test speed

The 'TRAIN Rig' moving-model facility consists of 150m long tracks along which model vehicles can be propelled at speeds of up to 75m/s. It is one of few aerodynamic facilities able to account for relative motion between vehicles, the ground, and complex structures such as train stations and tunnels. A simplified four-carriage 1/25 scale model ICE2 train was constructed, as shown in Fig. 1. The same train model and facility have been used in previous studies including Baker et al. (2001) and Temple and Dalley (2001), both of which provide datasets of open air transient slipstream measurements that are referred to in a comparison study in Section 3 of this paper. The former study also provides measurements of the model geometry. The test speed was 32m/s in order to match the test speed used in the former study for the benefit of the comparison study. The corresponding Reynolds number was 305,000 based on the speed and body height of the train (143mm at 1/25 scale).

The reduced Reynolds number of these experiments means that some inaccuracy due to the scale effect is unavoidable. In a CFD study on train wakes, Muld (2012) compared the boundary layer momentum thickness along the tail carriage of the simplified ICE2 with that of full-scale trains. This parameter affects the points of separation of the flow around the train's tail, and hence the flow structures in the wake. It was found that the modelled four carriage train had a momentum thickness equivalent to a full-scale train with 12 carriages. This suggests that despite the relatively short length of this train and the low test Reynolds

number, the wake flow structures are somewhat comparable to those occurring at full-scale in the open air. The data is compared with results from a previous full scale study in Section 3.

The speed of the model as it passed airflow measurement instruments was estimated from readings made by light gates stationed adjacently to the entrances and exits of the structures. 99% of the tested speeds were within 5.2% of the target speed of 32m/s. The uncertainty of the train speed measurement is 0.71%, based on a comparison between manually calculated speeds from recorded light gate data with automatically calculated speeds.

2.2 Geometry and flow variables

Positions and lengths in this paper are normalised by the train height. x/Z, y/Z, and z/Z are the longitudinal, lateral, and vertical directions, relative to the direction of travel, with x originating from the tip of the train's nose, y from the track centre, and z from the railhead. The full-scale equivalent dimensions of the train are X=105.4m (length), Y=3.075m (width), and Z=3.9m (height). The 1/25-scale dimensions of the train (as built) are X=4.216m, Y=0.123m, and Z=0.156m. Some useful reference values are defined: The positions of the nose and tail of the train are x/Z=0 and 27 respectively; the distance of the side of the train from the track centre is y/Z=0.39; the height of the top of the train above the top of the rail is z/Z=1; the height of the top of the rail above the ground is z/Z=0.077; and the rail heads are approximately y/Z=0.39 apart (1.535m at full-scale). The flow velocities in the longitudinal (u), lateral (v), and vertical (w) directions, and the resultant velocity (U), were converted into dimensionless coefficient forms with the train speed denoted by V. The dimensionless groups are as follows:

$$\left(\frac{x}{Z}\right)\ \left(\frac{y}{Z}\right)\ \left(\frac{z}{Z}\right)\ \left(\frac{u}{V}\right)\ \left(\frac{v}{V}\right)\ \left(\frac{w}{V}\right)\ \left(\frac{U}{V}\right)$$

Where:

$$\frac{U}{V}=\sqrt{\left(\frac{u}{V}\right)^2+\left(\frac{v}{V}\right)^2+\left(\frac{w}{V}\right)^2}$$

Two dimensionless variables are defined for the infrastructure. These are the blockage ratio β, which is the cross-sectional area of the train divided by that of the tunnel, and the leakage ratio, α, which is the ratio of the width of a gap in the cross-section of a tunnel divided by the total internal perimeter of a tunnel.

2.3 Test cases

Cross-section views and geometric details of the structures and instruments used in the tests are included in Fig. 2 and Table 1. The structures included a pair of walls (W1), single-track tunnels (T1, T1-B, T2, T3), and a partially-enclosed single-track tunnel (T2-P). Open air control experiments have also been carried out (OA). The standardised wall separation of y/Z=0.84 was chosen to allow a continuous walkway to theoretically run alongside the tracks, so worker access during train operation would be permitted for train speeds of 200kph in the UK (RSSB, 2011) or 160kph in Germany (EUK, 1999). The tunnel cases allowed the effect of changing tunnel length to be assessed, as well as α and β. The tunnel lengths were x/Z=51 (T1), 13 (T2), and 5 (T3), where β=0.23. The longest tunnel (T1) included a variation with a smaller cross-sectional area in which β=0.3 due to a lower ceiling height (T1-B). Tunnel T2 included a partially-enclosed variation (T2-P) in which α=4.3%, due to a slit running along the length of the ceiling. This particular α value represents the largest possible gap size within the limitations of the apparatus. Although three smaller gap sizes were tested for a concurrent

study on pressure transients (Gilbert et al., 2013), the velocity was not measured due to time constraints. Therefore only the largest gap size was tested. The tunnel cross sections were rectangular for two reasons. Firstly, it was possible to transition from vertical walls to tunnels by just installing a ceiling, therefore ensuring that one geometric variable was changed at a time. Secondly, the study on pressure transients required the use of rectangular tunnels.

2.4 Instrumentation and ensemble analysis

'TFI' Cobra Probes measured three components of flow velocity at various positions near the train. Results from three positions are included in this paper. Table 1 and Fig. 2 describe the positions of the probes, and the number of runs carried out for each test case. Probes C1 and C2 were positioned at identical heights, but C1 was situated close to the train's side and C2 was close to the wall, as can be seen in Fig. 2. Probes C2 and C3 were placed at near-identical lateral distances from the train's side, but at different heights. Probe C3 was placed close to the ground at a position which corresponds to the standing positions of trackside workers. .

The Cobra probes were calibrated by the manufacturer, and could detect maximum frequencies of 650Hz or 2000Hz (they came from two different batches). All data were low-pass filtered digitally. The filter parameters changed depending on the type of analysis, so they are disclosed in the results. Two types of filter are referred to in this work - a Butterworth low-pass filter and a moving-average filter. A fifth order Butterworth low-pass filter has been applied to the time history results, with a cutoff frequency equivalent to 0.1 seconds at full-scale. This cutoff frequency is based on the minimum recommendation made by Sterling et al. (2008) for risk assessing slipstream gust loads. The Butterworth filter was

applied in forward and reverse to prevent phase-shifting. The moving-average filter window was centred to prevent phase-shifting. The moving-average filter is referred to only in Section 5.2. Cobra probes have a 45 degree 'cone of acceptance' which limits their range of detection. Therefore the data from each individual scan is replaced with a zero (referred to as a 'dropout') if the flow angle exceeds an acceptable range of 45 degrees. Dropouts were highest around the nose and first carriage of the train. Dropouts were temporarily interpolated in the filtering process to prevent ripple in the time domain.

The manufacturer's uncertainty of the Cobra probes is 0.3m/s. This has been used in a propagation of error analysis to calculate the uncertainty of the maximum velocity normalised by train speed: two thirds of the maximum dimensionless velocities have uncertainties less than 2.9%, and five percent have uncertainties exceeding 5.2%.

Velocity time histories are highly turbulent for individual runs, so run-to-run variation must be accounted for using the 'ensemble averaging' technique to avoid over- or under-predictions. Schultz (1990) measured the transient slipstream velocity caused by a simplified moving-model ICE1 passing through short double-track tunnels of three different lengths. However, the tests were not repeated, so it was impossible to quantify the maximum velocity accurately. The technique has been employed in many recent studies of the flow in the open air, most notably Del Valle (2012). The technique involves repeating each test multiple times to form an 'ensemble' of N time histories. In this work, the sample axis was converted into a distance axis (x-axis, measured in x/Z), and the ensemble runs were aligned to a common point at the train's nose, so that $x/Z=0$ represented the train's nose passing the probe. Moreover, speed differences between runs caused the ensembles to go out of alignment with increasing absolute values of x/Z, so the data were re-sampled to align the ensemble time

histories to a common distance axis. The ensemble average was then obtained by calculating the average velocity for all samples at each increment on the distance axis.

The uncertainty of the ensemble average has been examined using data for three Cobra probes in T1. The 95% confidence limit of the standard deviation of the mean ($\sigma/\sqrt{N}$) for the maximum velocities in the ensemble was 2-2.8% for N=15, 1.5-1.9% for N=25, and 1.1-1.2% for N=40.

Table 1 provides details of the repeats completed for each probe and test case. N-values of higher than 40 were achieved by repeating measurements with longitudinally staggered Cobra probes, and low N-values occurred due to time constraints near the end of the test campaign.

Variables			**Test cases**						
			OA	**W1**	**T1**	**T1-B**	**T2**	**T2-P**	**T3**
Length	*x/Z*			51	51	51	13	13	5
Wall separation	*y/Z*			0.84	0.84	0.84	0.84	0.84	0.84
Ceiling height	*z/Z*				1.79	1.36	1.79	1.79	1.79
Leakage ratio	α (%)				0	0	0	4.3	0
Blockage ratio	β				0.23	0.3	0.23	0.23	0.23
Probe name	***y/Z***	***z/Z***	**Ensemble Repeats, *N***						
C1	0.48	0.58	60	25	40	25	16	16	15
C2	0.75	0.58	54	25	28	25	15	16	15
C3	0.77	0.05	62	50	40	25	16	15	15
Distance of probes from structure entrance (*x/Z*):				31	31	31	5	5	3

Table 1: Details of the probe positions, test case geometries, and number of runs carried out for each case.

3 Preliminary tests

Open air tests have been undertaken to check the ability of the methodology to recreate results from previous studies, and to check the reliability of the results. Fig. 3(a) shows the boundary layer profile measured by six Cobra probes, averaged along the third carriage and plotted against moving-model data from Baker et al. (2001). The study had used the same simplified ICE2 model, test speed, and track profile. Fig. 3(b) shows an open air wake time history plotted against full-scale and moving-model data from Temple and Dalley (2001). Hot-wire anemometers had been used in both of the moving-model studies. The methodology for the full-scale study differed considerably - gust anemometers had measured the slipstream of an eight-carriage ICE2 train on ballasted track. The results show that the velocities measured by the Cobra probes are the same or higher than those measured by hot-wire anemometers in the boundary layer region. Moreover, the ensemble average gust peak behind the train's tail is 12% lower than the full-scale measurement. However, the uncertainty of the ensemble average for the full-scale data was high, since the ensemble consisted of only seven runs. A two-sample t-test has been applied to the ensemble gust peaks to determine whether the difference between these results and full-scale results are significant to the $p \leq 0.05$ level. The p-value is 0.23, meaning that the differences are unlikely to be statistically significant.

To further evaluate the reliability of the results, the open air experiments have been repeated. Two-sample t-tests have been applied to ensemble velocity time histories and velocity maxima. The tests revealed that the maximum velocities are likely to come from the same

statistical distributions, with p-values ranging from 0.13 to 0.55 for the four repeated experiments. The differences between ensemble averages have been found by comparing whether the ensemble velocities come from the same statistical distributions. The only significant differences occur in the nose region in which near-inviscid flow reduces the standard deviation considerably. A further reliability test involved staggering two probes along the x-axis and taking double measurements for given test cases. The differences between the maximum velocities are likely to be insignificant, with p-values ranging from 0.25 to 0.37. The differences between the time histories were insignificant. In conclusion, it is presumed that this methodology is acceptable in relation to previous accepted methodologies for similar reduced-Reynolds number tests in the open air, which gives increased confidence in the results for confined cases.

4 Results

4.1 Open air flow field

Fig. 4 shows fundamental flow structures around the ICE2 in the open air, based on measurements in past studies. Fig. 4(a) is a surface representation of the results from moving-model tests reported in Baker et al. (2001). The boundary layer begins to grow along the second carriage ($x/Z>6.7$), and appears to reach a constant thickness by $x/Z=20$. Gust peaks occur around the train's nose and tail. Fig. 4(b) is from a CFD study by Hemida et al. (2012), showing a time-averaged two-dimensional quiver plot of a dominant flow structure in the near-wake of a simplified ICE2. The flow structure comprises helical vortices which are alternately shed from the left and right sides of the train's tail, causing powerful velocity transients. Although not visible in either figure, at low-heights the near-wake is also dominated by a coherent peak in longitudinal velocity, which extends far from the train's side in the lateral axis. At greater heights, such as in Fig. 4(a), the near-wake is dominated by separated shear layers, in which the velocity decays quickly in comparison to the low-height measurements.

Open air data from these experiments is shown in Fig. 5. It may be regarded as control data against which to compare the confined results. The ensemble average data for Probe C1 shows high velocities in the boundary layer region, due to the close proximity of the probe to the train's side. For Probes C2 and C3, the velocities in the boundary layer region are low, due to their greater lateral separations from the train's side. A high-magnitude peak velocity occurs at low heights in the near-wake region, and has been captured by Probe C3. The peak

gusts are denoted by markers. They are clustered in the boundary layer region for Probe C1 and in the wake for Probes C2 and C3.

4.2 Walls

Fig. 6 shows the results for vertical walls. The velocity in the boundary layer region is very similar to that in the open air at all probe positions. However, the decay of the velocity in the near-wake region is much more gradual, which prolongs the gust duration. For Probe C1, a larger proportion of the peak gusts occur in the near-wake region compared to the open air. The data for Probe C2 shows that the ensemble average peak velocity in the near-wake region is approximately three times higher than the open air. All of the peak gusts occur in the near-wake region. The data for Probe C3 is only available in the near-wake region. It shows a small increase in the magnitude of the ensemble average peak velocity, relative to the open air, combined with a slower decay after the peak. These results suggest that the constraint caused by the walls most significantly affects the flow in the near-wake, causing stronger low-height gusts than in the open air, the effects of which are detected at higher positions.

4.3 Tunnels

As a train enters a tunnel, a number of relevant pressure phenomena occur. Firstly a pattern of pressure waves is set up by compression and expansion wave-fronts which reflect internally from the entrance and exit portals of the tunnel, causing rapid pressure changes. Secondly, a ‘piston effect’ is induced by the combined effects of compression of the air ahead of the train’s nose and expansion behind the train’s tail. This is characterised by a sustained velocity occurring ahead of the train’s nose and slowly decaying far behind the tail. Third of all, the

flow pattern takes a finite time to change after entering the confined space. The combination of the aforementioned phenomena creates a complex flow pattern which is not repeatable at any different location in the tunnel and cannot be perfectly recreated in reduced scale tests. These results must be regarded as a qualitative indication of the flow patterns in tunnels.

Fig. 7 shows the results for fully-enclosed tunnels of three lengths. The results for T1-B are omitted because the flow patterns are similar to T1. In the region between the train's nose entering the tunnel and reaching the probe, a fluctuation occurs due to a passing compression wavefront, and then the velocity increases as a favourable pressure gradient is created in the direction of the tunnel exit. The effect is more noticeable in the longer tunnels. In T1-B, β is 30% higher than T1, and the peak velocity in the nose region is approximately 40% higher. The piston-effect is the dominant flow structure causing this increase, as it is fundamentally related to blockage ratio, and also because other localised flow changes due to moving the boundaries were minimised by using only the ceiling height to control β - the ceiling was far from the probes. Moving on to the boundary layer region, the obvious difference compared to the open air is that the ensemble average velocity in the longest tunnel is noticeably lower and the thickness of the boundary layer is reduced. This finding is backed up by observations by Sakuma et al. (2010) of the boundary layer around a train in a tunnel. The form parameter (H) may provide firmer confirmation. Although estimating H is inaccurate with just four probes (two of which are not mentioned elsewhere in this paper, but were located between Probes C1 and C2 on the y-axis), changes between test cases may be significant. H is defined by:

$$H = \frac{\int U\, dy/Y}{\int U(1-U)\, dy/Y}$$

In T1-B, H stabilises from the second carriage to the tail, reaching 1.1, which is lower than 1.2 which was calculated for the open air and wall results. This decrease indicates a boundary layer typical of a less favourable pressure gradient. In the shorter tunnels, the ensemble average and spatial distribution of the gust peaks for Probe C1 in the boundary layer region are closer to those seen in the results for the walls. This suggests that the decreased length of the tunnel and the corresponding reduction in the distance of the probes from the tunnel entrance act as key variables in determining the flow patterns in the boundary layer region. Moving on to the near-wake region, the velocity in the longest tunnel is higher than that recorded in the wall case. As the tunnel's length reduces, the gust peaks detected by Probe C1 shift towards the boundary layer region, showing a convergence with the results for the open air and walls. Interestingly, the ensemble average peak for Probe C3 in T3 is higher than that in T2. This appears to be caused by a tighter spatial distribution of the gust peaks, rather than an increase in velocity magnitudes. The results are analysed further in Section 5.

4.4 Partially-enclosed tunnel

Fig. 8 shows the results for T2-P, which is a partially-enclosed variant of T2 in which α=4.3%. The flow patterns in the nose region remain similar to those in T2, but the flow patterns in the boundary layer region are similar to those in the less confined wall and open air cases. In the near-wake region, the locations and magnitudes of the gust peaks are more tightly distributed, causing higher ensemble average peak magnitudes. The results for Probe C2 show a high near-wall velocity (Probe C2). This is analysed further in Section 5.

5 Discussion

5.1 Velocity components in the near-wake

This section will explore the contribution of each velocity component to the resultant velocity peaks, by deconstructing the ensemble average velocity data presented in Section 4 into the longitudinal, lateral and vertical components. Only the near-wake region is considered, because it is a critical region in which hazardous gusts occur, and the results suggest that the flow patterns in this region are the most sensitive to the parametric changes studied. Fig. 9 shows the data for the open air (OA), tunnels of two lengths (T1 and T2), and the partially-enclosed tunnel (T2-P). A Butterworth low-pass filter smoothed the data further to a cut-off frequency equivalent to 0.25 seconds, to make interpretation easier at the expense of minor peak attenuation.

The results show that confinement causes the longitudinal velocity to increase to a similar magnitude at all probe positions, which for Probe C2 represents a great change compared to the open air results. This observation may be due to the piston effect, as the pressure and velocity changes associated with this effect are near-one-dimensional. The longitudinal velocity component, and hence the piston effect, may therefore be a dominant cause of the increased wake velocity peak magnitudes in the confined cases. By comparison, the lateral and vertical velocity components, which are associated with the helical vortex structures in the near-wake region, do not appear to have much influence on the results. The longitudinal velocity is higher in T2-P than in T2, which suggests that a small opening in the cross-section

of the tunnel is not sufficient to dissipate the piston-induced flow sufficiently to reduce the maximum transient gust velocity in the wake region.

The lateral velocity does not change significantly between cases. However, the results for Probes C1 and C2 show a stronger peak magnitude of vertical velocity in T2-P than in T2. The greatest increase occurs close to the wall surface (Probe C2). The opening in the ceiling may be responsible for inducing the high vertical velocity towards or away from the opening, depending on the instantaneous pressure difference between the tunnel and the surrounding environment. This would explain why the results for Probe C2 in Fig. 8 show a higher ensemble average velocity peak than the other probes. We may conclude that the lateral and vertical velocity only increase in certain circumstances, and also that Probe C3 did not detect any significant changes in these velocity components due to its close proximity to constraining boundaries.

5.2 Low height gusts in confined spaces

In this section, statistical gust analysis methodologies have been applied to the velocity data. Gust analysis methods are typically used for assessing transient dynamic loads on objects, or risk assessing the safety of passengers and trackside workers. An EU-wide 'TSI' code for high-speed trains (CEN, 2008) imposes limit criteria on the slipstream loads acting on trackside workers. The limit criteria must be met by all high-speed rolling stock operating across national borders under interoperability legislation. A methodology is defined in the TSI code (referred to herein as the 'TSI methodology') for assessing conformance to the limit criteria, but it stipulates open air operation only. The lack of a methodology for assessing gusts in tunnels provides an opportunity to try different approaches, two of which are used in

this section. Both methods rely on results for Probe C3, which was placed in the 'TSI position'. The first method, the 'TSI method', used a 1 second window moving-average filter to smooth each individual run, and followed the TSI methodology requirements as closely as possible. The second method, the '0.1 second method', relied instead on a fifth order Butterworth low-pass filter with a cutoff frequency corresponding to 0.1 seconds, which is the same filter that was used in the time history graphs presented earlier. The latter method was used to account for the inherent problem of over-smoothing in the TSI method, which is an effect discussed in Baker et al. (2013b). As explained previously, 0.1 seconds is the minimum recommended filter window size for risk assessing slipstream gust loads. Both methods relied on calculating the mean and standard deviation σ of the values of the peak gusts, of which there were N for each test case (see Table 1), and $U_{2\sigma}$:

$$U_{2\sigma} = \bar{u} + 2\sigma$$

Discussion in Baker et al. (2013b) reveals that this statistical approach is valid based on analysis of full-scale open air experimental data. Therefore $U_{2\sigma}$ may be interpreted as the 5% probability level gust. Table 2 shows the results of this assessment. Extra columns show $U_{2\sigma}$ converted to units of metres per second by multiplying $U_{2\sigma}$ by the ICE2 operational speed of V=280kph, so the velocity may be compared with the TSI gust limit of 22m/s.

Test case	Runs, N	TSI method				0.1s method			
			σ	$U_{2\sigma}$	$U_{2\sigma}$ (m/s)		σ	$U_{2\sigma}$	$U_{2\sigma}$ (m/s)
OA	62	0.21	0.04	0.29	22	0.32	0.085	0.49	38
W1	50	0.25	0.028	0.3	24	0.35	0.068	0.49	38
T1	40	0.3	0.037	0.38	29	0.44	0.067	0.58	45
T1-B	25	0.32	0.042	0.4	31	0.52	0.096	0.72	56
T2	16	0.25	0.024	0.29	23	0.37	0.067	0.51	39
T2-P	15	0.26	0.027	0.31	24	0.42	0.048	0.51	40
T3	15	0.24	0.031	0.3	24	0.37	0.061	0.49	38

Table 2: Gust analysis results for all test cases.

Firstly, the open air $U_{2\sigma}$ value is compared with results from a previous study. The flow around a double-unit (16 carriages) ICE2 was measured at full-scale in accordance with the TSI methodology, and was reported in Baker et al. (2013b). $U_{2\sigma}$ was found to be between 0.27 and 0.28. The finding in this study of 0.29 is in close agreement. The small difference may be explained by different experimental approaches and levels of uncertainty.

The results show that the highest values of $U_{2\sigma}$ occur in the longest tunnels. The shorter tunnels have similar $U_{2\sigma}$ values to the open air. Assessment of the regularity of exceedence of the gust limit based on the probability distributions generated by the TSI method reveals that $U_{2\sigma}$ in the short tunnels exceeds the gust limit two to three times more regularly than the open air, even in the shortest tunnel. It cannot therefore be assumed that no change in $U_{2\sigma}$ equates to no change in risk. $U_{2\sigma}$ in T2-P is very similar to that in T2, but the limit is exceeded three times more regularly than in T2.

The differences in the results between the TSI method and the 0.1s method are due to the relationship between the filter width and the gust length scale, which affects the gust peak attenuation. The gust magnitude limit should be varied accordingly with the filtered gust duration. The 22m/s limit is clearly not relevant when the filter design differs from that required in the TSI methodology. We may conclude that the cut-off frequency is an important consideration in designing a risk assessment methodology for confined flows, both in terms of the predicted gust magnitude and the relative changes between test cases. The probability of limit exceedence is more capable than $U_{2\sigma}$ for distinguishing which test cases cause higher risks than others.

5.3 Velocity in the far wake

In tunnels, the velocity in the far-wake region provides a level of natural ventilation. This section compares the far-wake velocity results between test cases. Fig. 10(a) shows the ensemble average velocity in the far-wake region, for the open air (OA) case, and tunnels of three lengths (T1-T3). The results show that the ensemble average velocity in the shortest tunnel is similar to that in the open air - the velocity is initially high but decays rapidly. The velocity in the longest tunnel remains high long after the train has passed. This behaviour is likely to be a specific feature of the piston effect. Fig. 10(b) shows that in the high blockage ratio tunnel (T1-B), the velocity is highest close to the centre of the tunnel cross-section (Probe C1), and lowest in the lower corner (Probe C3) - a finding which is repeated for the other cases. Further analysis reveals that in the confined cases, the wake velocity reaches 1m/s (for V=280kph) three to four times further from the rear of the train than in the open air.

6 Conclusions and further work

Moving-model experiments have been carried out to measure the transient slipstream velocity caused by a simplified ICE2 train model passing walls, single-track tunnels of varying lengths and cross-sectional areas, and a partially-enclosed tunnel which was formed by creating an opening in the ceiling of a tunnel through which air could enter and leave. An open air control experiment was carried out. From the analysis in the previous sections, the following conclusions can be drawn:

(a) An assessment of the maximum transient gust velocity at the 5% probability level, for a low-height trackside position, reveals that vertical walls close to the train increase the maximum gust velocity compared to the open air. Relative increases also occur as a result of: transitioning from walls to tunnels; increasing the length of a tunnel; decreasing the cross-sectional area of a tunnel; and creating an opening to form a partially-enclosed tunnel. In all of these confined cases, gusts occur over a longer duration than in the open air. The combined increases in gust durations and magnitudes may result in exceptionally high loads on objects.

(b) In tunnels, a high longitudinal airflow occurs upstream of the train's nose and in the wake due to a piston effect - a simple flow structure which moves the internal air column within a tunnel in a near-one-dimensional manner. The magnitude of the peak piston-induced velocity is dependent on tunnel length and cross-sectional area. It has been found to be a dominant cause of very high gust loads in the near-wake region, at all positions inside tunnels, due to its superposition with lateral and vertical velocity peaks. It is also responsible for the reduced rate of decay of the velocity which extends the durations of the maximum gusts as well as the time taken for the air to return to ambient conditions, which affects the ventilation characteristics of tunnels.

(c) When a partially-enclosed tunnel is formed by creating a small opening in a tunnel, high velocities occur in the direction of the opening in the wake region. This causes the resultant gust velocity to increase relative to enclosed tunnels. The highest gusts occur close to the walls due to vertical flow, which may result in exceptionally high gust loads on near-wall objects.

(d) In calculating a characteristic gust for comparing different confined spaces, and which may be used for assessing risks caused by gust loads, two low-pass filtering methodologies have been compared. The characteristic gust magnitude varies significantly due to the different levels of attenuation of the gust peaks caused by the filters. Filter design is therefore a crucial consideration in carrying out such assessments. Moreover, for some test cases the characteristic gusts were very similar, but a different parameter based on the regularity of limit exceedence revealed significant differences between them.

(e) Preliminary open air experiments were carried out. Repeated experiments and measurements produced time histories which closely corresponded with each other along most of the train, and the peak velocities were found to come from the same statistical distribution. The peak velocities in the open air appear to come from the same statistical distribution as one calculated for results from a past full-scale study, despite an average velocity peak 12% lower than full-scale. It may be concluded that this methodology is acceptable and the results for confined spaces are likely to be reliable.

In future work, the effect of changing the train's geometry should be tested so we may understand whether these observations hold for trains with different aerodynamic shapes. Some of the observations are difficult to interpret without taking into account the pressure

field around the train, so further work is needed to interpret the relationship between pressure gradients and the boundary layer and wake flows. Moreover, some transient flow patterns have not been identified in this paper, as they are hidden by the ensemble averaging technique. Therefore, the individual runs from this dataset should be analysed further.

Acknowledgements

The authors are indebted to Dr. Sarah Jordan, David Soper and Martin Gallagher from the University of Birmingham, for their help with performing the moving-model experiments.

References

Busslinger, A., Hagenah, B., Reinke, P., Rudin, C., 2009. Aerodynamics and climate in the Loetschberg base tunnel - prediction and findings. In: ITA-AITES World Tunnelling Congress, Budapest, Hungary, 23-28 May.

Baker, C.J., Dalley, S.J., Johnson, T., Quinn, A., Wright, N.G., 2001. The slipstream and wake of a high speed train. Proceedings of the Institution of Mechanical Engineers Part F: Journal of Rail and Rapid Transit, 215, 83-99.

Baker, C.J., 2001. Flow and dispersion in ground vehicle wakes. Journal of Fluids and Structures, 15, 1031-1060.

Baker, C.J., Quinn, A., Sima, M., Hoefener, L., Licciardello, R., 2013a. Full scale measurement and analysis of train slipstreams and wakes: Part 1 Ensemble averages. Proceedings of the Institution of Mechanical Engineers Part F: Journal of Rail and Rapid Transit, doi:10.1177/0954409713485944.

Baker, C.J., Quinn, A., Sima, M., Hoefener, L., Licciardello, R., 2013b. Full scale measurement and analysis of train slipstreams and wakes: Part 2 Gust analysis. Proceedings of the Institution of Mechanical Engineers Part F: Journal of Rail and Rapid Transit, doi: 10.1177/0954409713488098.

CEN, 2003. Railway applications - Aerodynamics - Part 3: Aerodynamics in tunnels, CEN EN 14067-3:2003.

CEN, 2006. Railway applications - Aerodynamics - Part 5: Requirements and test procedures for aerodynamics in tunnels. CEN EN 14067-5:2006 +A2:2010.

CEN, 2008. EU Technical Specification For Interoperability Relating to the 'Rolling Stock' Sub-System of the Trans-European High-Speed Rail System, Directive 96/48/EC, 2008/232/EC, 2008.

Del Valle, N., 2012. Measurement and analysis of slipstreams for passenger trains. Doctoral thesis, University of Birmingham.

Deutsche Bahn, 2003. Eisenbahntunnel planen, bauen und instand halten. Regelwerk D853, August 2003.

EUK, 1999. Arbeiten im Bereich von Gleisen. GUV-V D 33. EUK-Dialog 6.99.

Gilbert, T., Baker, C. & Quinn, A. 2013b. Aerodynamic pressures around high-speed trains: the transition from unconfined to enclosed spaces. Accepted for publication in Proceedings of the Institution of Mechanical Engineers Part F: Journal of Rail and Rapid Transit.

Hemida, H., Baker, C.J., Gao, G., 2012. The calculation of train slipstreams using Large Eddy Simulation. Proceedings of the Institution of Mechanical Engineers Part F: Journal of Rail and Rapid Transit, doi:10.1177/0954409712460982.

Krajnovic, S., 2009. Large eddy simulation of flows around ground vehicles and other bluff bodies, Philosophical Transactions of the Royal Society A, 367, 2917-2930.

Krajnovic, S., Bjerklund, E., Basara, B., 2009. URANS of the flow around high-speed trains meeting each other and at the exit of a tunnel. In: 21st International Symposium on Dynamics of Vehicles on Roads and Tracks, Stockholm, Sweden, 17-21 August.

Muld, T., 2012. Slipstream and flow structures in the near-wake of high-speed trains. Doctoral thesis, KTH Royal Institute of Technology.

RSSB, 2011. Handbook 1: General duties and track safety for track workers. GE/RT8000/HB1 Iss 1.

Sakuma, Y., Suzuki, M., Ido, A., Kajiyama, H., 2010. Measurement of air velocity and pressure distributions around high-speed trains on board and on the ground. Journal of mechanical systems for transportation and logistics, 3(1), 110-118.

Schultz, M., 1990. Experimentelle und rechnerische Ermittlung von Druckwellenausbreitungsvorgängen bei der Fahrt eines Zuges durch einen kurzen Tunnel. Unterschung des Einflusses der instationären Wandreibung auf die Wellendämpfung. PhD Thesis, Technischen Universität Wien.

Sterling, M., Baker, C.J., Jordan, S.C., Johnson, T. 2008. A study of the slipstreams of high-speed passenger trains and freight trains. Proceedings of the Institution of Mechanical Engineers Part F: Journal of Rail and Rapid Transit, 222(2), 177-193.

Temple, J., Dalley, S., 2001. RAPIDE Project: Analysis of the slipstream data, AEA Technology Rail, Report number AEATR-T&S-2001-197, 2001.

Figure captions

Fig. 1. Photograph of the simplified ICE2 model.

Fig. 2. Cross-section views and photographs of the test structures. All dimensions are common to W1, apart from the height of T1-B.

Fig. 3. Validation against previous moving-model and full-scale experiments: (a) Boundary layer profile along the third carriage, using data from Baker et al. (2001); (b) Time history of the wake, using data from Temple and Dalley (2001).

Fig. 4. Velocity data for the ICE2 train from past studies. (a) Surface plot on an x-y plane, showing the velocity next to the train side. Adapted from Baker et al. (2001); (b) Time-averaged quiver plot of the secondary velocity components in the near wake (Hemida et al., 2012).

Fig. 5. Open air: Ensemble average and ensemble peaks of the resultant velocity for Probes C1 to C3.

Fig. 6. Walls (W1): Ensemble average and ensemble peaks of the resultant velocity for Probes C1 to C3.

Fig. 7. Tunnels: (a) T1 (longest); (b) T2; (c) T3 (shortest). Ensemble average and ensemble peaks of the resultant velocity for Probes C1 to C3.

Fig. 8. Partially-enclosed tunnel (T2-P): Ensemble average and ensemble peaks of the resultant velocity for Probes C1 to C3.

Fig. 9. The longitudinal (u/V), lateral (v/V) and vertical (w/V) velocity components in the near wake, for four test cases, for Probes C1 to C3.

Fig. 10. Ensemble average of the resultant velocity in the far wake for different: (a) Test cases; (b) Measurement positions in tunnel T1-B.

FIG1

Click here to download high resolution image

FIG2

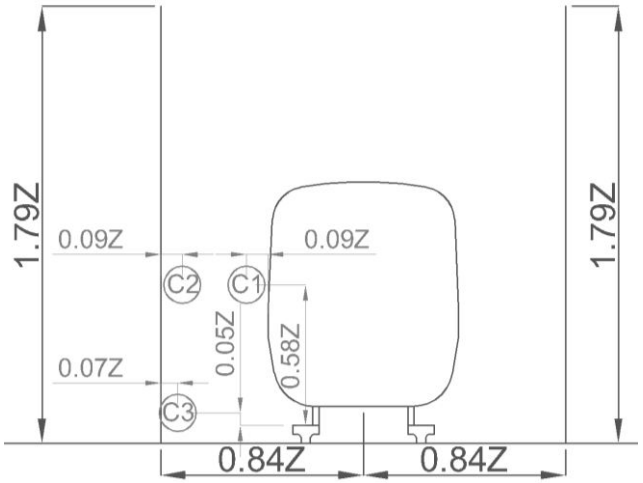

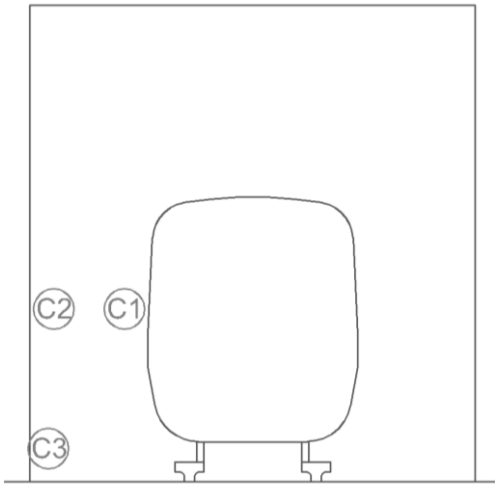

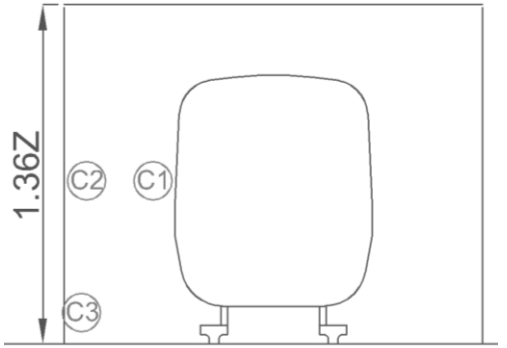

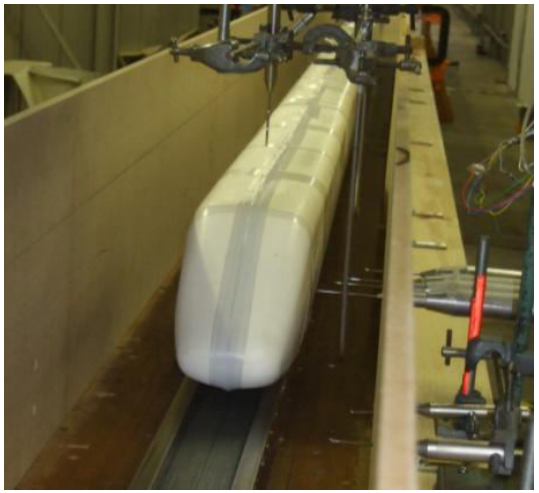

W1

T1, T2, T2-P, T3 (pictured).

T1-B

FIG3

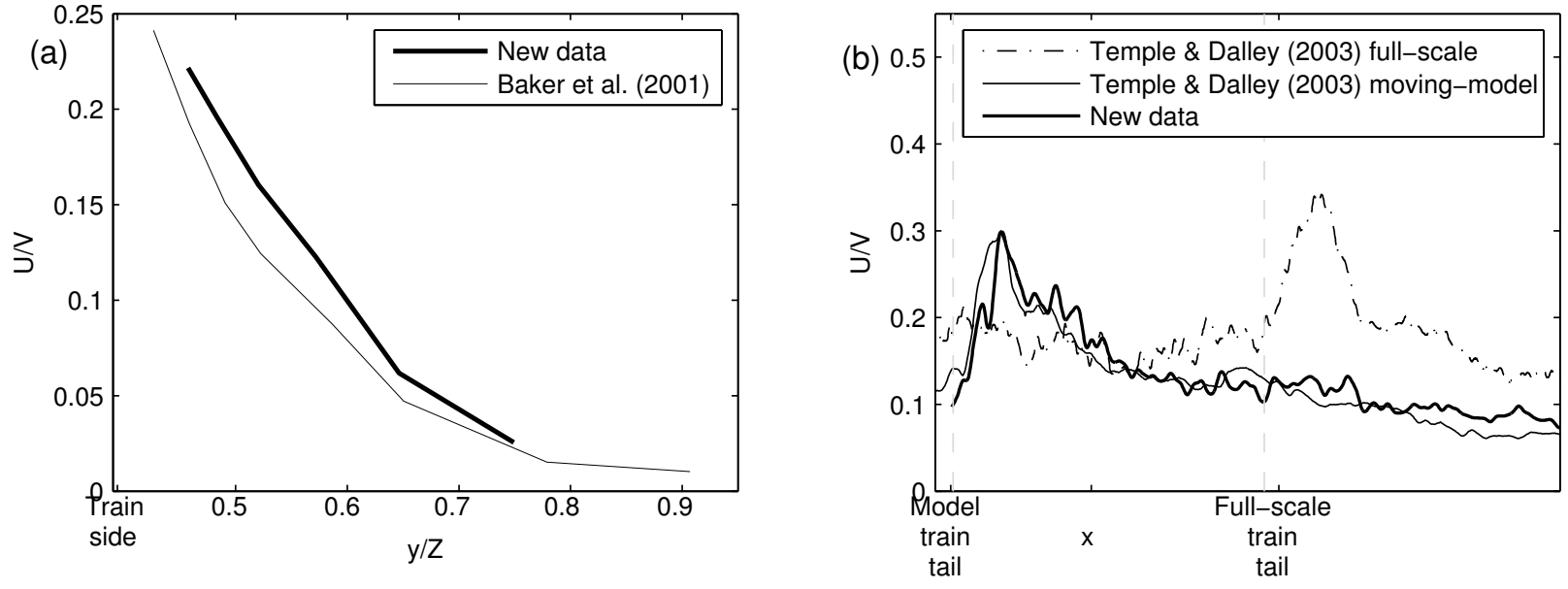
(a)
New data
Baker et al. (2001)
U/V
y/Z
Train side
0.25
0.2
0.15
0.1
0.05
0
0.5
0.6
0.7
0.8
0.9
(b)
Temple & Dalley (2003) full−scale
Temple & Dalley (2003) moving−model
New data
U/V
x
Model train tail
Full−scale train tail
0.5
0.4
0.3
0.2
0.1
0

FIG4

Click here to download high resolution image

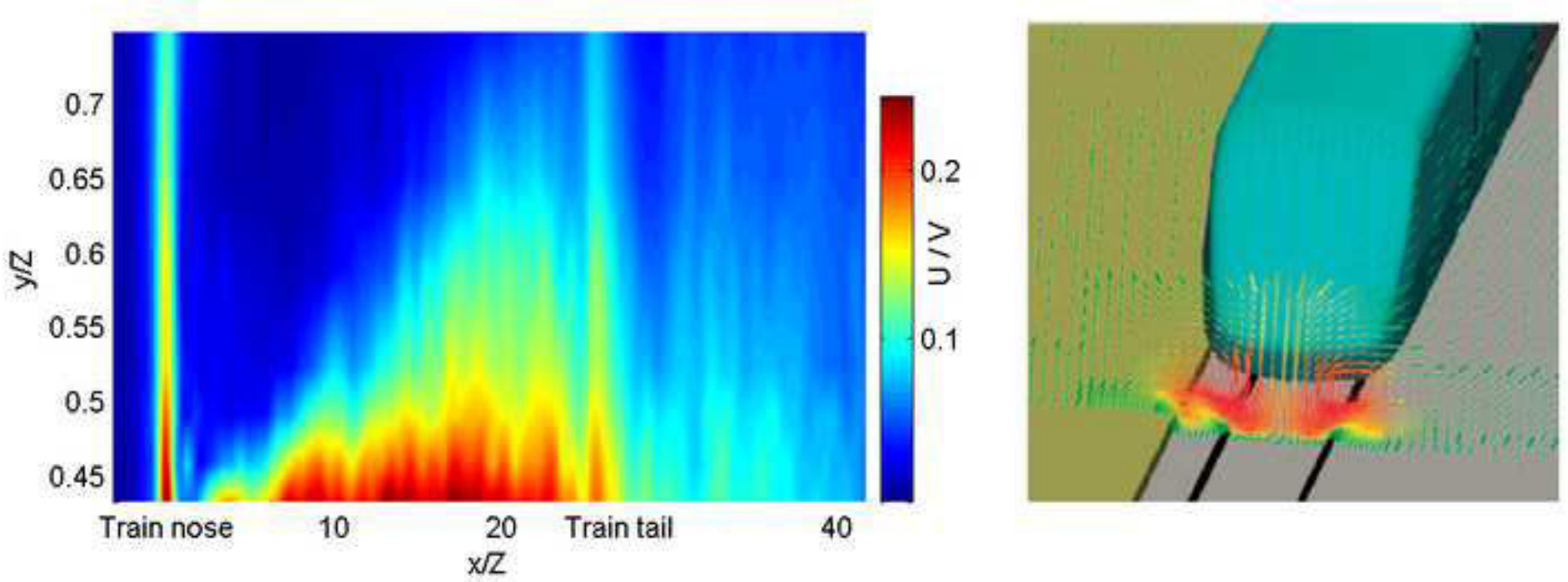

FIG5

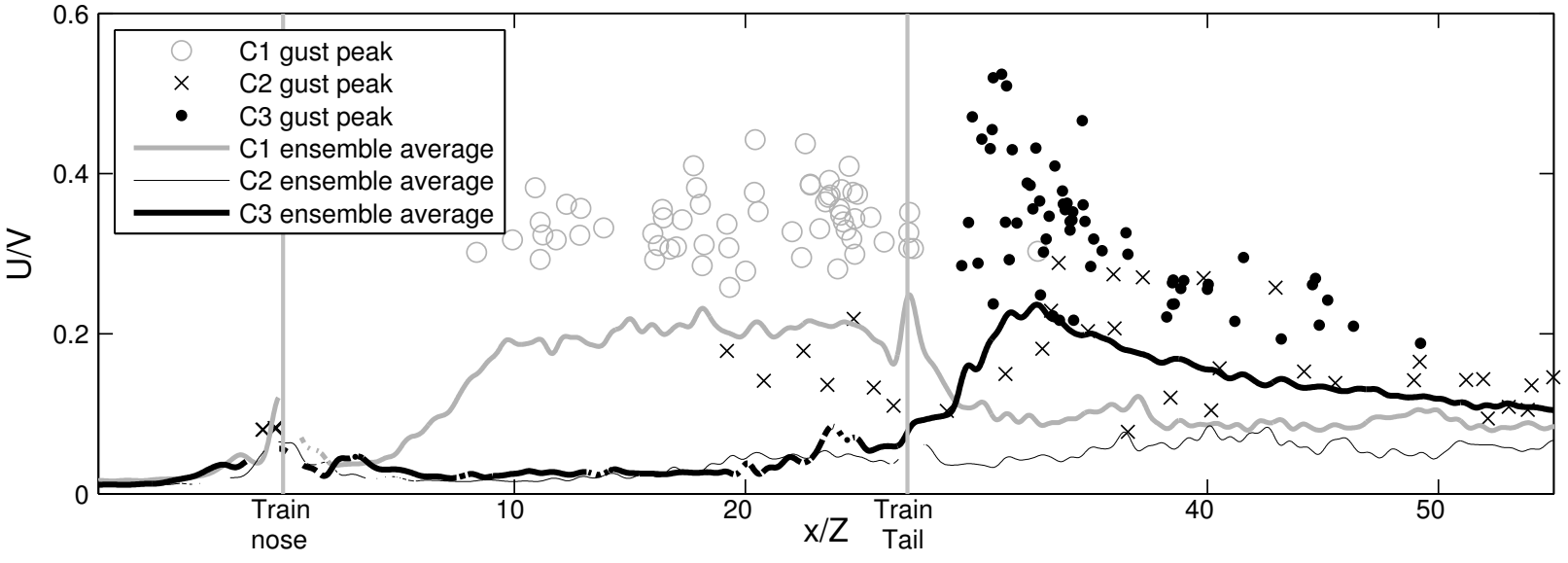
C1 gust peak
C2 gust peak
C3 gust peak
C1 ensemble average
C2 ensemble average
C3 ensemble average
U/V
0.6
0.4
0.2
0
Train nose
10
20
x/Z
Train Tail
40
50

FIG6

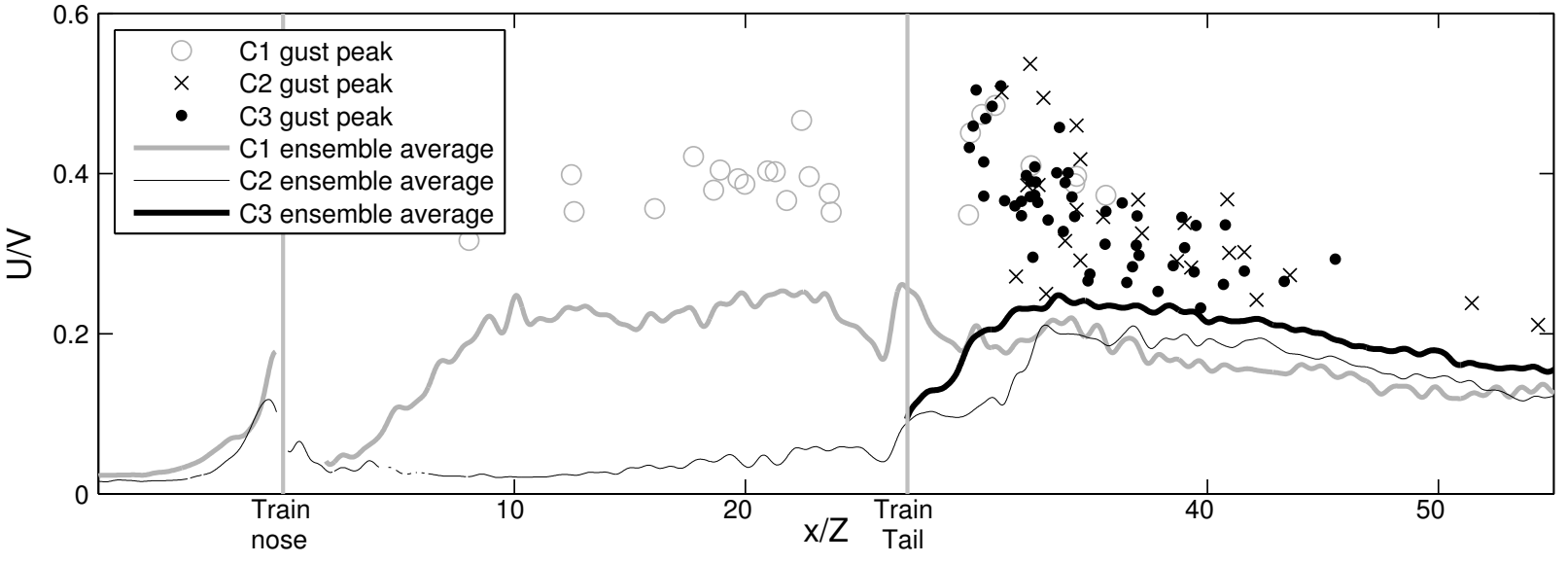
C1 gust peak
C2 gust peak
C3 gust peak
C1 ensemble average
C2 ensemble average
C3 ensemble average
U/V
0.6
0.4
0.2
0
Train nose
10
20
x/Z
Train Tail
40
50

FIG7

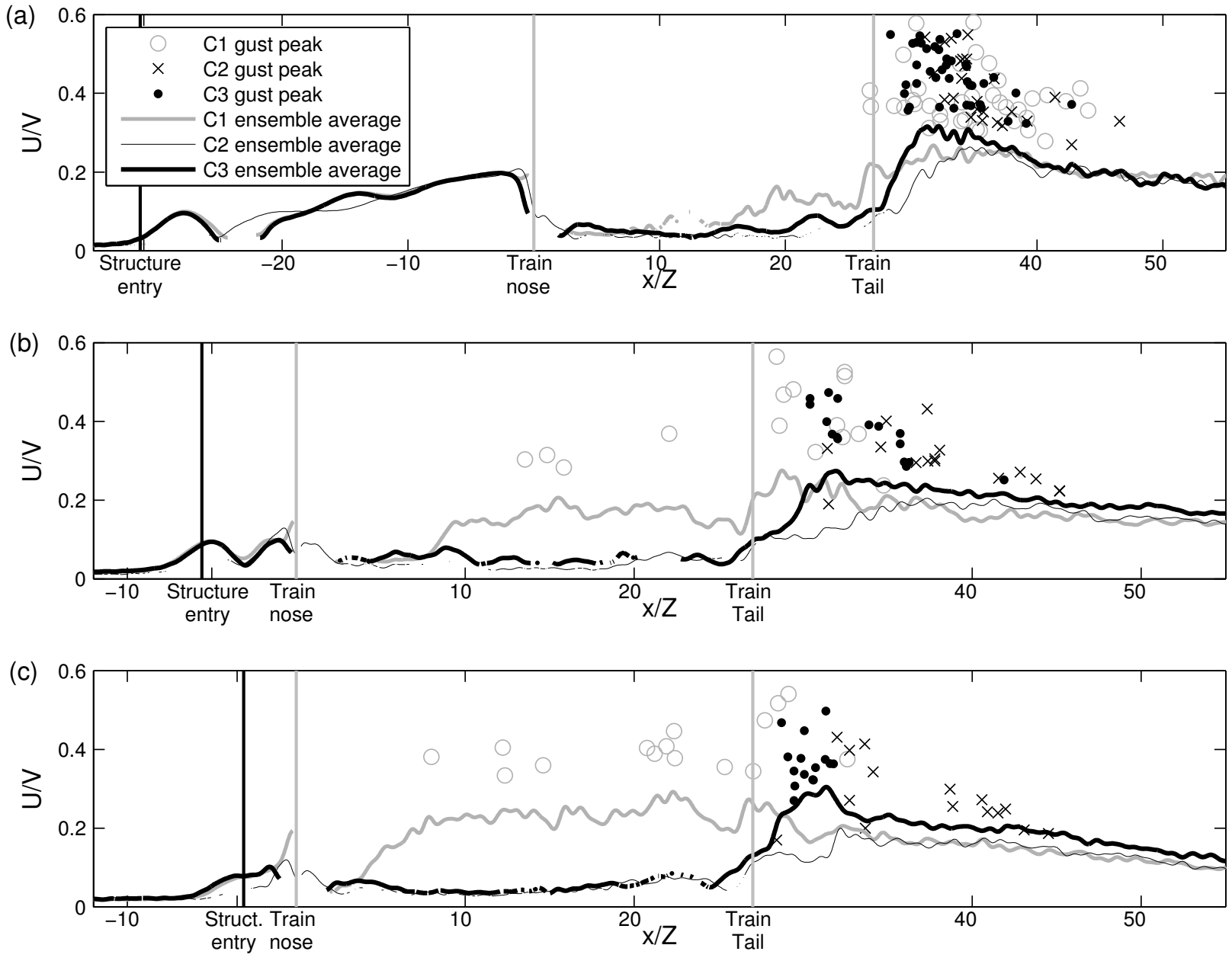
(a)
C1 gust peak
C2 gust peak
C3 gust peak
C1 ensemble average
C2 ensemble average
C3 ensemble average
U/V
0.6
0.4
0.2
0
Structure entry
−20
−10
Train nose
10
20
Train Tail
40
50
x/Z
(b)
U/V
0.6
0.4
0.2
0
−10
Structure entry
Train nose
10
20
Train Tail
40
50
x/Z
(c)
U/V
0.6
0.4
0.2
0
−10
Struct. entry
Train nose
10
20
Train Tail
40
50
x/Z

FIG8

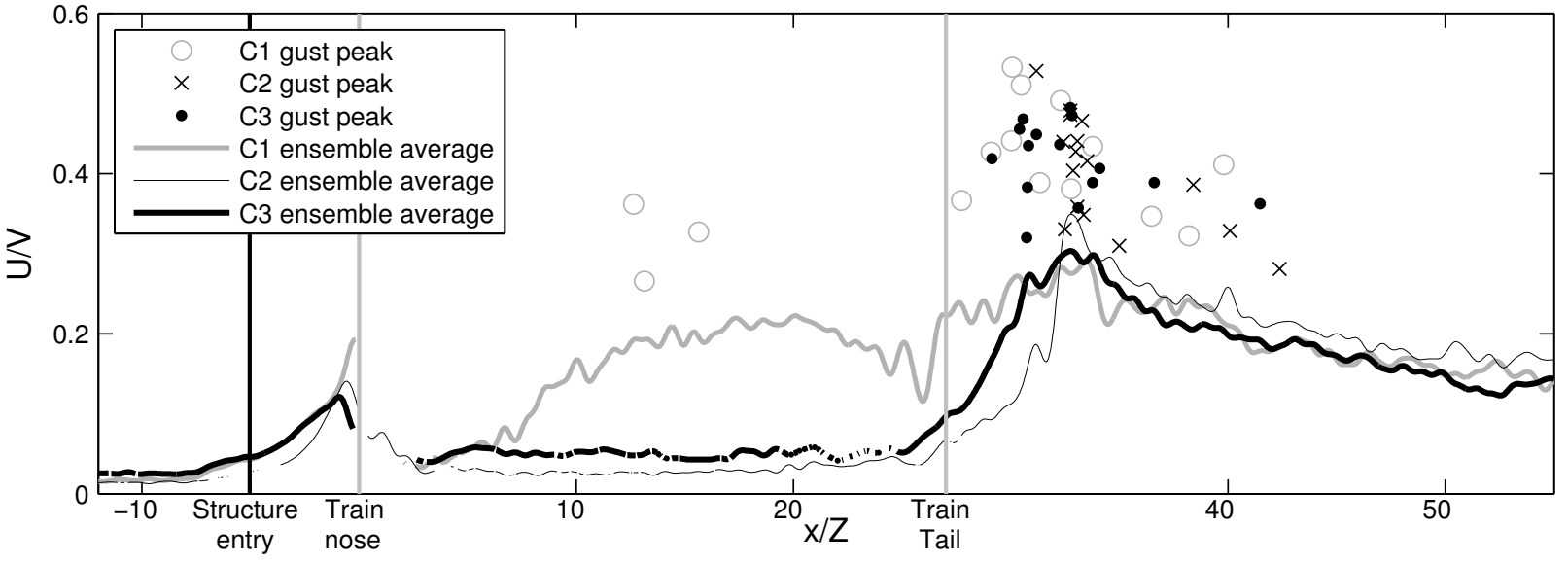
C1 gust peak
C2 gust peak
C3 gust peak
C1 ensemble average
C2 ensemble average
C3 ensemble average
U/V
0.6
0.4
0.2
0
−10
Structure entry
Train nose
10
20
x/Z
Train Tail
40
50

FIG9

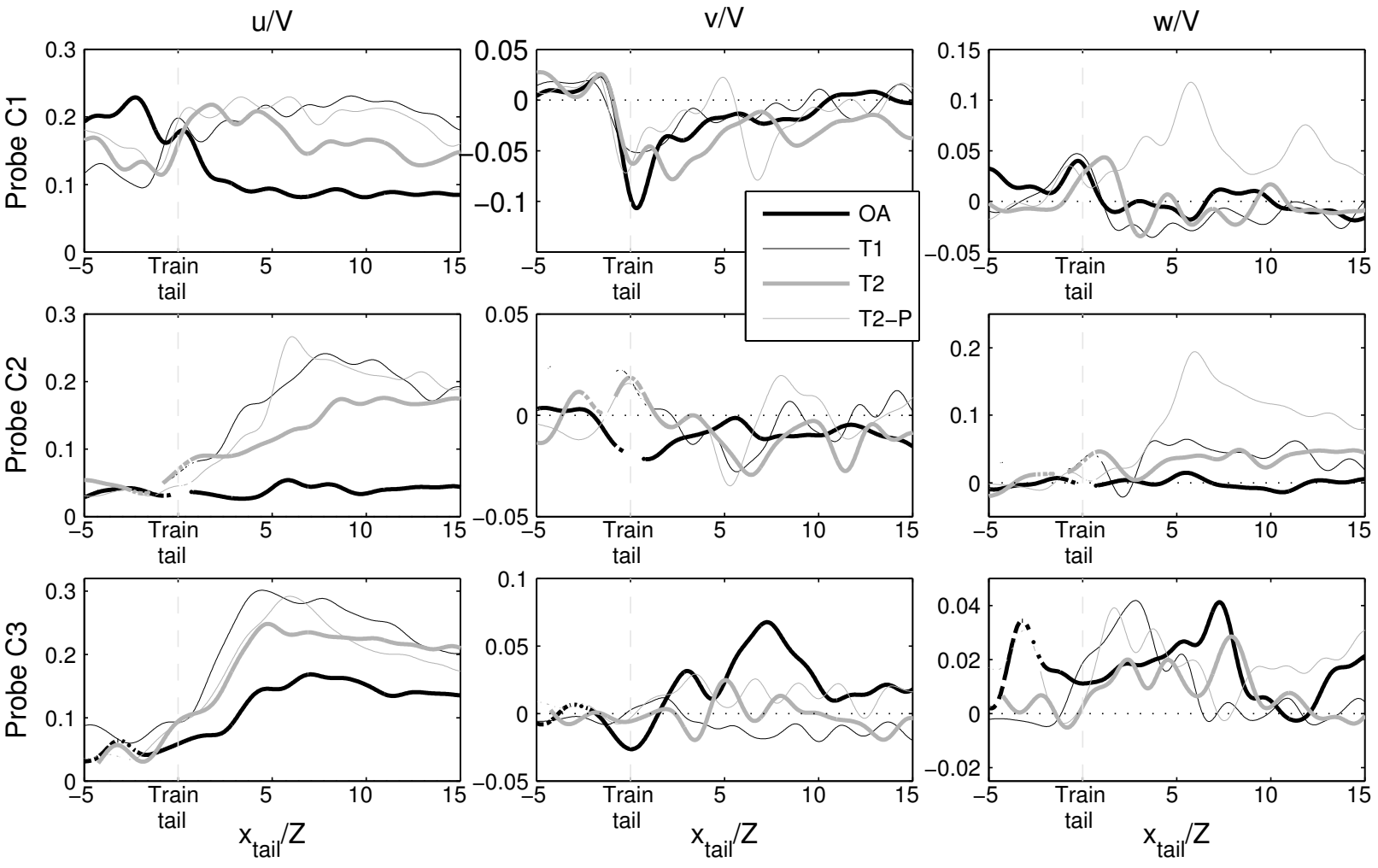
u/V
v/V
w/V
Probe C1
Probe C2
Probe C3
OA
T1
T2
T2−P
Train
tail
x_{tail}/Z

FIG10

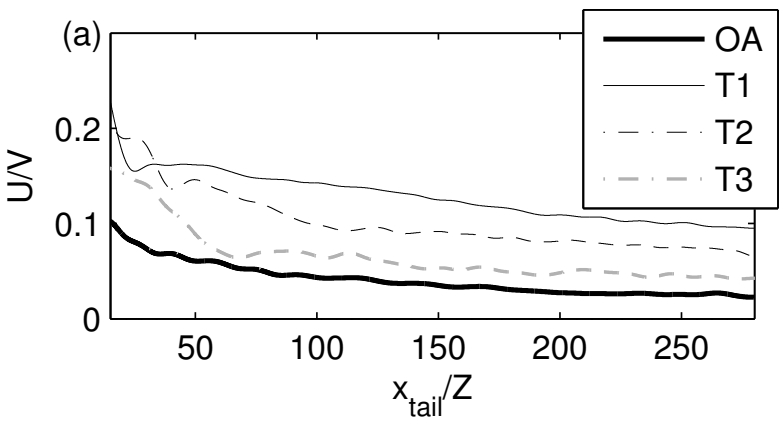
(a)
OA
T1
T2
T3
U/V
0
0.1
0.2
50
100
150
200
250
x_tail/Z

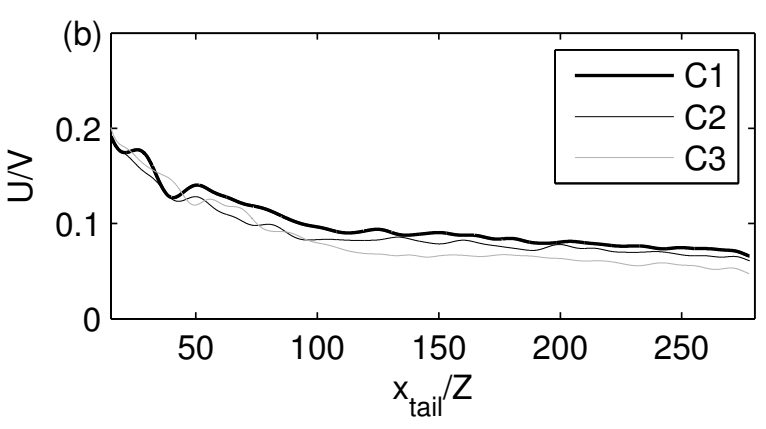
(b)
C1
C2
C3
U/V
0
0.1
0.2
50
100
150
200
250
x_tail/Z